Alfvén waves and ideal two-dimensional Galerkin truncated magnetohydrodynamics

Giorgio Krstulovic,[1,2] Marc-Etienne Brachet,[1] and Annick Pouquet[3]

[1]*Laboratoire de Physique Statistique de l'École Normale Supérieure, associé au CNRS et aux Universités Paris VI et VII, 24 Rue Lhomond, F-75231 Paris, France*

[2]*Laboratoire Cassiopée, Observatoire de la Côte d'Azur, CNRS, Université de Nice Sophia-Antipolis, Boulevard de l'Observatoire, F-06300 Nice, France*

[3]*Computational and Information Systems Laboratory, National Center for Atmospheric Research, P.O. Box 3000, Boulder, Colorado 80307-3000, USA*

(Received 5 January 2011; revised manuscript received 20 April 2011; published 28 July 2011)

We investigate numerically the dynamics of two-dimensional Euler and ideal magnetohydrodynamics (MHD) flows in systems with a finite number of modes, up to 4096^2, for which several quadratic invariants are preserved by the truncation and the statistical equilibria are known. Initial conditions are the Orszag-Tang vortex with a neutral X point centered on a stagnation point of the velocity field in the large scales. In MHD, we observe that the total energy spectra at intermediate times and intermediate scales correspond to the interactions of eddies and waves, $E_T(k) \sim k^{-3/2}$. Moreover, no pseudodissipative range is visible for either Euler or ideal MHD in two dimensions. In the former case, this may be linked to the existence of a vanishing turbulent viscosity whereas in MHD, the numerical resolution employed may be insufficient. When imposing a uniform magnetic field to the flow, we observe a lack of saturation of the formation of small scales together with a significant slowing down of their equilibration, with however a cutoff independent partial thermalization being reached at intermediate scales.

DOI: 10.1103/PhysRevE.84.016410 PACS number(s): 52.65.Kj, 47.27.Ak, 05.20.Jj

I. INTRODUCTION

A theory of turbulent flows is still eluding us, and yet such flows are ubiquitous in nature and are an integral part of the problem of weather prediction or of climate assessment, as well as for the formation and prediction of extreme events such as tornadoes and hurricanes; they are also an important element in the understanding of the dynamics of planets and the heliosphere, stars and beyond. What is lacking is a statistical description of the small scales, and a prediction of long-time large-scale dynamics with ensuing modified transport properties. Of course, since Onsager (1949) [1], who considered an ensemble of point vortices in two space dimensions (2D), and T. D. Lee (1952) [2], who pioneered the study of the behavior of a truncated system of modes for both inviscid fluids and ideal magnetohydrodynamics (MHD) in three dimensions (3D), we have known that equipartition of energy among the modes obtains in the simplest (3D, nonhelical) case, whereas spectra peaking at the gravest mode in the 2D case are possible; these latter solutions can be viewed as precursors of inverse cascades toward large scales, observed in 2D for forced dissipative fluids and for MHD [3,4] (see [5] for a review), as well as in 3D MHD [6] (see [7] for a review). Numerous extensions of the 2D problems introducing potential vorticity lead to the same prediction of an inverse cascade of energy, as in the quasigeostrophic case.

It has been argued that inviscid dynamics is in fact a good indicator of the behavior of turbulent flows in the presence of forcing and dissipation. This is certainly the case for scales larger than the forcing scale $\ell_F = 2\pi/k_F$ when an inverse cascade is present, but evidence for scales smaller than ℓ_F has been lacking until recently. It was shown, using high-resolution ideal runs in 3D for Euler flows, that at intermediate times and intermediate scales, a Kolmogorov energy spectrum (hereafter, K41), $E(k) \sim k^{-5/3}$, is observed, as well as a pseudodissipative range at the end of the K41 spectrum; note that by pseudodissipation, we mean that no actual dissipation takes place globally in such ideal flows; the latter range can be attributed to an eddy viscosity acting on low-k modes due to the thermalized high-k modes, $E(k) \sim k^2$ [8] (see also [9] in the helical case when velocity-vorticity correlations are included, and [10] in the 3D rotating case, with or without helicity). One of the most striking results on the truncated Euler equations is thus that the thermalized zone progressively extends to large scales finally covering the whole spectrum as expected, but that the intermediate scales are found to follow an effective Navier-Stokes equation [9,11] even though dissipation is absent.

Two-dimensional MHD is special for at least two reasons. First, the 2D ideal fluid case possesses an infinite number of invariants, even though only the quadratic ones are being preserved in the truncated system. Nevertheless, the aforementioned predictions of inverse cascades have been verified in many instances [5]: One can indeed argue that other invariants, such as any power of the vorticity field integrated over space, will be dissipated efficiently in the realistic case in which forcing and viscosity are included. Furthermore, in MHD, there is a controversy as to what is the energy spectrum in the forced dissipative case: It could be a classical Kolmogorov spectrum, either isotropic or anisotropic, in the latter case with a dependence on $k_\perp$ (referring to the direction perpendicular to an imposed strong uniform magnetic field $\mathbf{b}_0$, of magnitude b_0 [12]). Or it could be an Iroshnikov-Kraichnan spectrum (hereafter, IK [13,14]) stemming from the interactions of Alfvén waves and turbulent eddies and leading to the slowing down of the nonlinear cascade when waves are strong; in fact, this latter solution is compatible with the prediction of weak turbulence theory for MHD [15] when the resulting spectrum is isotropized. Moreover, it has been argued by several authors

that there is no complete universality in MHD, including in the absence of forcing and with $\mathbf{b}_0 \equiv 0$ (see [16] and references therein).

In this paper, we thus investigate the properties of ideal two-dimensional MHD and Euler flows. The next section explains the procedure we follow and recalls several known properties of ideal 2D MHD; in Sec. III, we give results in the absence of imposed magnetic field, $\mathbf{b}_0 \equiv 0$. In Sec. IV, we analyze the slowing down of the dynamics for $\mathbf{b}_0 \neq 0$; finally, Sec. V briefly examines the structures that develop in space, and Sec. VI is the conclusion. The special ($\mathbf{b} = 0$) Euler case in two dimensions is treated in the Appendix.

II. THE PROCEDURE

We begin by writing the ideal MHD equations in the incompressible case ($\nabla \cdot \mathbf{u} = 0$, where $\mathbf{u}$ is the velocity field) by introducing a pseudoscalar potential $\psi(x,y,t)$, the stream function, and the (scalar) magnetic potential $a(x,y,t)$, with $\mathbf{u} = \nabla \times \psi$ and $\mathbf{b} = \nabla \times a$, $\mathbf{b}$ being the magnetic induction, also divergence-free ($\nabla \cdot \mathbf{b} = 0$) in the absence of magnetic monopoles:

$$\frac{\partial \psi}{\partial t} = \frac{1}{\nabla^2}\{\psi, \nabla^2 \psi\} - \frac{1}{\nabla^2}\{a, \nabla^2 a\}, \tag{1}$$

$$\frac{\partial a}{\partial t} = \{\psi, a\}, \tag{2}$$

where $\{f,g\} = \partial_x f \partial_y g - \partial_x g \partial_y f$ is the usual Poisson bracket. Regrouping some terms in Eq. (2), it can be shown that the magnetic potential also satisfies

$$\frac{\partial a}{\partial t} + \mathbf{u} \cdot \nabla a = 0, \tag{3}$$

and therefore a is advected as a passive scalar by the fluid, even though the Lorentz force $\mathbf{j} \times \mathbf{b}$ acts on the fluid and breaks the conservation of vorticity in 2D (with $\mathbf{j} = \nabla \times \mathbf{b}$ the current density). Equations (1) and (2) conserve the total energy

$$E = \frac{1}{2} \int d^2x \, [|\mathbf{u}|^2 + |\mathbf{b}|^2]; \tag{4}$$

they also have an infinite number of conserved quantities, the Casimirs, of the form

$$\mathcal{C} = \int d^2x \, [f(a) + \nabla^2 \psi g(a)], \tag{5}$$

where f and g are arbitrary functions. Among them, two remarkable invariants are obtained for $f(a) = a^2$, $g(a) = 0$ and for $f(a) = 0$, $g(a) = -a$; the former one, denoted $A \equiv \langle a^2 \rangle$, is the conserved square magnetic potential and the latter is called the cross helicity which can also be written as $H_c = \int d^2x \, \mathbf{b} \cdot \mathbf{u}$. As remarked in [5], the invariants in MHD do not go over smoothly into the conserved quantities of the hydrodynamics equations, except for total energy. We can expect then a different behavior, even if the magnetic field is weak initially.

The truncated MHD equations for the pair of Fourier modes $\psi_{\mathbf{k}}$ and $a_{\mathbf{k}}$, with $k \in [k_{\min}, k_{\max}]$, are defined in a similar way to the truncated Euler equation:

$$\frac{\partial \psi_{\mathbf{k}}}{\partial t} = \frac{1}{k^2} \sum_{\mathbf{p},\mathbf{q}} (\mathbf{p} \times \mathbf{q}) q^2 [\psi_{\mathbf{p}} \psi_{\mathbf{q}} - a_{\mathbf{p}} a_{\mathbf{q}}] \delta_{\mathbf{k},\mathbf{p}+\mathbf{q}}, \tag{6}$$

$$\frac{\partial a_{\mathbf{k}}}{\partial t} = -\sum_{\mathbf{p},\mathbf{q}} (\mathbf{p} \times \mathbf{q}) \psi_{\mathbf{p}} a_{\mathbf{q}} \delta_{\mathbf{k},\mathbf{p}+\mathbf{q}}, \tag{7}$$

with $\delta_{\mathbf{k},\mathbf{r}}$ the Kronecker delta and with Fourier modes satisfying $\psi_{\mathbf{k}} = 0$, $a_{\mathbf{k}} = 0$ if $|\mathbf{k}| \geqslant k_{\max}$; for a computational box of length 2π, we have $k_{\min} = 1$, and with a de-aliasing using the usual 2/3 rule, $k_{\max} = N/3$, where N is the number of modes per dimension (we assume a box with a unit aspect ratio).

This truncated system only conserves the quadratic invariants, which can be written in Fourier space as

$$E = \frac{1}{2} \sum_{\mathbf{k}} |\mathbf{u}_{\mathbf{k}}|^2 + |\mathbf{b}_{\mathbf{k}}|^2, \tag{8}$$

$$H_c = \sum_{\mathbf{k}} \mathbf{u}_{\mathbf{k}} \cdot \mathbf{b}_{-\mathbf{k}}, \tag{9}$$

$$A = \frac{1}{2} \sum_{\mathbf{k}} |a_{\mathbf{k}}|^2. \tag{10}$$

The truncated dynamics Eqs. (6) and (7) will first (but only as long as spectral convergence is ensured) give an accurate approximation of the solution to Eqs. (1) and (2), see below Fig. 2 and the discussion preceding Eq. (24). The truncated dynamics is then expected to reach, at much later times, an absolute equilibrium that is a statistically stationary Gaussian exact solution of the associated Liouville equation [17]. At intermediate times, the modes may thermalize between some transition wave number and the maximum wave number, see below Fig. 3. In the 3D Euler case, it was shown in [8] that the thermalized modes can act as a fictitious microworld providing an effective dissipation to the modes with wave numbers below the transition wave number.

The absolute equilibrium corresponds to the equipartition distribution of the following combination of invariants (as first derived in [18], see also [5]) $\alpha E + \beta A + \gamma H_c$, where α, β, and γ are Lagrange multipliers (note that H_c is not definite positive and that γ is a pseudoscalar). This leads to the following equilibrium spectra:

$$E_u(k) = \frac{\pi k}{\mathcal{D}} [k^2 \alpha + \beta], \tag{11}$$

$$E_b(k) = \frac{\pi k}{\mathcal{D}} k^2 \alpha, \tag{12}$$

$$H_c(k) = -\frac{2\pi k}{\mathcal{D}} k^2 \gamma, \tag{13}$$

with

$$\mathcal{D} = k^2(\alpha^2 - \gamma^2) + \alpha\beta.$$

For small values of β, we have equipartition of kinetic and magnetic energy $E_u(k) = E_b(k) \sim \pi k \alpha/(\alpha^2 - \gamma^2)$ at all scales.

In the presence of a constant magnetic field aligned with the x axis $\mathbf{b_0} = b_0 \hat{x}$, Eqs. (1) and (2) are modified by performing

TABLE I. Time step dt for the various ideal MHD numerical simulations presented in this paper. In all cases, the total energy is conserved at better than 0.1% at the final time of the computation T_f. Note that $b_{\rm rms} \sim 2.5$ when $b_0 \equiv 0$, so that all cases have a dominant imposed field b_0, except the one with $b_0 = 0$ and $b_0 = 2$.

Run	N^2, T_f	$\mathbf{b}_0 = 0$	$\mathbf{b}_0 = 2$	$\mathbf{b}_0 = 4$	$\mathbf{b}_0 = 8$	$\mathbf{b}_0 = 12$	$\mathbf{b}_0 = 16$
1	256^2, $T_f = 500$						$dt = 1/16000$
2	512^2, $T_f = 60$	$dt = 1/1600$	$dt = 1/3200$	$dt = 1/3200$	$dt = 1/6400$	$dt = 1/8000$	$dt = 1/8000$
3	2048^2, $T_f = 20$	$dt = 1/20000$					
4	2048^2, $T_f = 5$		$dt = 1/10000$	$dt = 1/20000$	$dt = 1/40000$		$dt = 1/40000$
5	4096^2, $T_f = 1.2$	$dt = 1/20000$					

the substitution $a \to a + b_0 y$. The MHD equations thus become

$$\frac{\partial \psi}{\partial t} = \frac{1}{\nabla^2}\{\psi, \nabla^2 \psi\} - \frac{1}{\nabla^2}\{a, \nabla^2 a\} + b_0 \partial_x a, \tag{14}$$

$$\frac{\partial a}{\partial t} = \{\psi, a\} + b_0 \partial_x \psi. \tag{15}$$

With $\mathbf{b}_0 \neq 0$, the square magnetic potential $A = \langle a^2 \rangle$ is no longer conserved and the absolute equilibrium spectra given in Eqs. (11)–(13) are obtained in this case by setting $\beta = 0$. For small amplitudes, Eqs. (14) and (15) lead to the wave equation $\partial_{tt}^2 b_y = b_0^2 \partial_{xx}^2 b_y$ with the Alfvén wave relation dispersion $\omega(\mathbf{k}) = b_0 k_x = \mathbf{b_0} \cdot \mathbf{k}$.

Note that 2D statistical equilibria for a neutral fluid in the compressible (adiabatic) case are derived analytically in [19] and that compressible 2D MHD was analyzed numerically in the context of long-time relaxation in [20]. Both of these papers examine the relative dominance of vortical to acoustic modes; in particular, a dependence on the initial data, both in MHD and for neutral fluids, is observed [21], because of different asymptotic regimes.

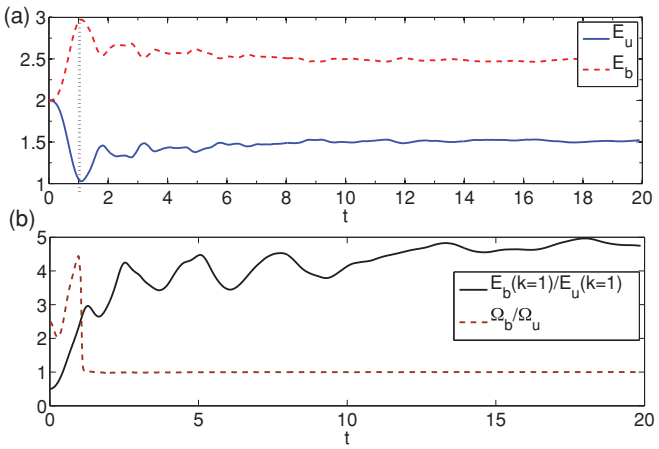

FIG. 1. (Color online) (a) Temporal evolution of kinetic and magnetic energy, E_u (in solid blue) and E_b (in dashed red) for a run at a resolution of 2048^2 grid points (run 3, $b_0 \equiv 0$); the dashed vertical line indicates the final time of the numerical integration reported in [23] on 512^2 grid points. (b) Temporal evolution of $E_b(k=1)/E_u(k=1)$ (solid line) and of total enstrophies $\Omega_b/\Omega_u = \langle j^2 \rangle / \langle \omega^2 \rangle$ (dashed red line) for the same run. As long as the large-scale ($k \sim 1$) modes have not equilibrated, nonlinear transfer to the magnetic energy persists whereas equipartition is reached rapidly in the small scales, as indicated by the long plateau in Ω_b/Ω_u.

III. THERMALIZATION IN THE ABSENCE OF A UNIFORM MAGNETIC FIELD

A. The Orszag-Tang configuration in 2D MHD

In order to study the thermalization of ideal MHD in two dimensions through a direct cascade of energy to small scales, we now resort to a numerical study. The code is a standard pseudospectral code with periodic boundary conditions; the temporal scheme is a Runge-Kutta time stepping of fourth order that is known to accurately conserve the energy. The time steps used in our computations are given in Table I; note that they are substantially lower than the CFL condition so that energy can be preserved by the scheme for long times.

We take as initial conditions the so-called Orszag-Tang (OT) vortex in 2D defined by the potentials [22]:

$$\psi(x,y) = 2(\cos k_0 x + \cos k_0 y), \tag{16}$$

$$a(x,y) = 2\cos k_0 x + \cos 2k_0 y; \tag{17}$$

with $k_0 = 1$, this vortex, made up of a neutral X point for the magnetic field centered on the stagnation point of the velocity field, is concentrated in the large scales with $E_u = E_b = 2.0$ at $t = 0$; hence, the initial rms values of the turbulent fields are $u_{\rm rms} \sim b_{\rm rms} \sim 2$.

The short time dynamics is identical to the one studied in [23] at a resolution of $N^2 = 512^2$ Fourier modes and until the final time $T_f = 1$. Here, we integrate the truncated MHD equations until $T_f = 20$ using a grid of $N^2 = 2048^2$ points. Note that the structures that develop at early times in physical space, namely a quadrupole in vorticity and a current dipole, were studied in detail in [23] and are only briefly commented upon in Sec. V.

The temporal evolution of the kinetic and magnetic energy is shown in Fig. 1: There is at first an energy exchange between the kinetic energy (blue, solid line) and the magnetic energy (red, dashed line), with the magnetic energy dominating its kinetic counterpart except at $t \equiv 0$. As thermalization is reached, after a time ~ 5, the exchanges die out since the thermalized solution has no nonlinear energy flux; E_b/E_u settles at ~ 1.7, leading to $u_{\rm rms} \sim 1.5$, $b_{\rm rms} \sim 2.5$. Such a moderate excess of magnetic energy is often observed in the solar wind [24]; it corresponds to a slight departure from equipartition that can be attributed, in the context of ideal flows, to the effect of the conservation of the magnetic potential, see Eqs. (11) and (12). We define as usual the total

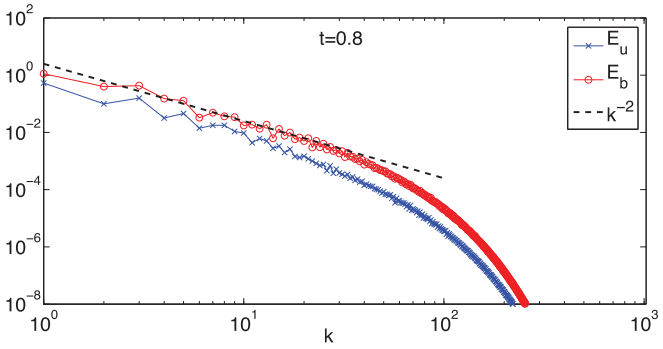

FIG. 2. (Color online) Kinetic (×, blue) and magnetic (circle, red) energy spectra at $t \sim 0.83$, in the early phase of the flow for run 3 with $b_0 \equiv 0$ (see Table I). The black dashed line corresponds to k^{-2}, a spectrum expected in the presence of quasisingular structures. Note that magnetic energy dominates at all scales at that time.

energy and total enstrophy spectra by summing the basic fields on circular shells of width $\Delta k = 1$:

$$E_T(k,t) = \frac{1}{2} \sum_{k_- < |\mathbf{k}'| < k_+} [|\hat{\mathbf{u}}(\mathbf{k}',t)|^2 + |\hat{\mathbf{b}}(\mathbf{k}',t)|^2], \quad (18)$$

$$\Omega_T(k,t) = \frac{1}{2} \sum_{k_- < |\mathbf{k}'| < k_+} [|\hat{\omega}(\mathbf{k}',t)|^2 + |\hat{\mathbf{j}}(\mathbf{k}',t)|^2, \quad (19)$$

with $k_\pm = k \pm \Delta k/2$; $\hat{\mathbf{u}}(\mathbf{k},\mathbf{t})$, $\hat{\omega}(\mathbf{k},t)$, $\hat{\mathbf{b}}(\mathbf{k},\mathbf{t})$, and $\hat{j}(\mathbf{k},\mathbf{t})$ are the Fourier transforms of the velocity, vorticity, magnetic field, and current density, with $j_z = \nabla \times \mathbf{b}\hat{e}_z$. In Fig. 1(b), the ratio of the kinetic and magnetic energy spectra at $k = 1$ (black solid line) is displayed, as well as the ratio $\langle j^2 \rangle / \langle \omega^2 \rangle$ (corresponding to the ratio of kinetic and magnetic dissipation when equal viscosity and resistivity are reintroduced in the equations, red dashed line). Observe that magnetic energy dominates at large scale, a sign of a plausible inverse cascade associated with the magnetic potential and confirming that the defect in equipartition is indeed due to the large-scale behavior of the system, since almost exact equipartition is observed at small scale (see, e.g., Fig. 3).

Concerning spectral variations, at early times as displayed in Fig. 2, the spectra show a clear k^{-2} dependence, which can be associated with the formation of quasisingular current and vorticity sheets [23]. This behavior is exhibited by all spectra: kinetic (blue ×), magnetic (red circle), and total energy. It is also present (data not shown) when a uniform magnetic field is imposed on the flow, granted its magnitude is not too large compared to the rms values of the fluctuating field: For $b_0 = 0.5$, a similar spectrum obtains whereas for $b_0 = 4$, the spectrum is much steeper, due in part to a slower dynamical evolution (see next section). This k^{-2} spectrum associated with sharp current and vorticity sheets persists as long as convergence of the partial differential equations is assured, i.e., until the thickness of current and vorticity structures is comparable (but still larger) than the grid size [see also the discussion concerning the logarithmic decrement displayed in Fig. 6(a)].

It was shown in [8] in the context of three-dimensional ($D = 3$) Euler flows that, as time evolves, another dynamics takes place: Once the flow behaves as a truncated system of modes and thermalization begins, the modes following a k^{D-1} law at small scale for the three-dimensional Euler equations produce an eddy viscosity for larger scales; a quasiturbulent regime follows at intermediate scales and intermediate times (i.e., before thermalization occurs everywhere), with an inertial range close to a Kolmogorov law corresponding to the forced dissipative case.

Similarly in the present 2D case, once the smallest resolved scale has been reached, the overall solution becomes noisier, the vorticity and current sheets curve and interact, and the Fourier spectra evolve as well (structures are displayed in Fig. 9 below).

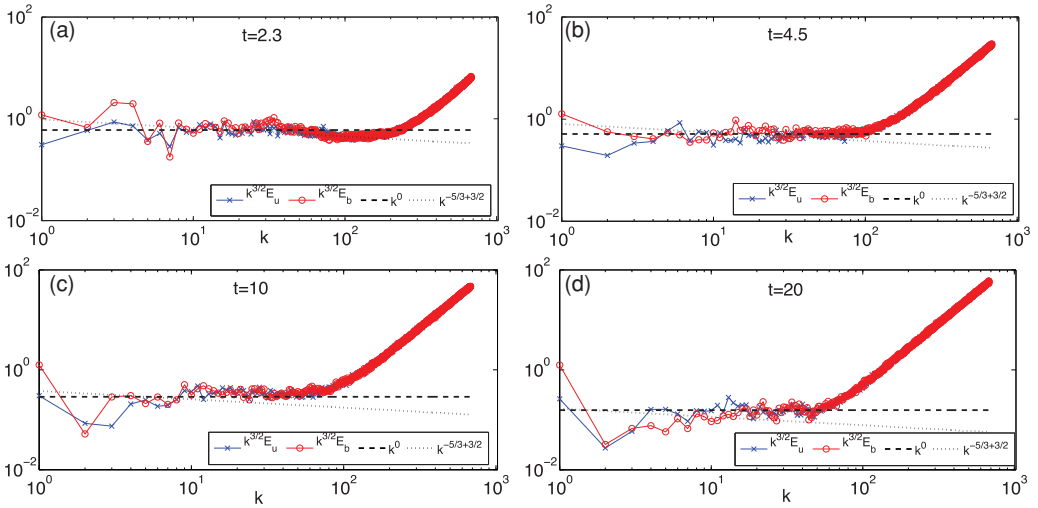

FIG. 3. (Color online) (a) to (d): Energy spectra for various times, compensated by $k^{3/2}$ (IK spectrum, see text): kinetic (×, blue) and magnetic (circle, red). Dashed and dotted lines represent fit for the K41 and IK solutions, respectively, the constants appearing in these spectra being fixed at the earliest time shown, $t \approx 2.3$. Grid of 2048^2 points, for run 3 with $b_0 \equiv 0$ (see Table I). Note the fast equipartition [$E(k) \sim k$] at small scale, the IK spectrum for more than one decade at intermediate scales and intermediate times, and the persistence for long times of the domination of magnetic energy at large scale.

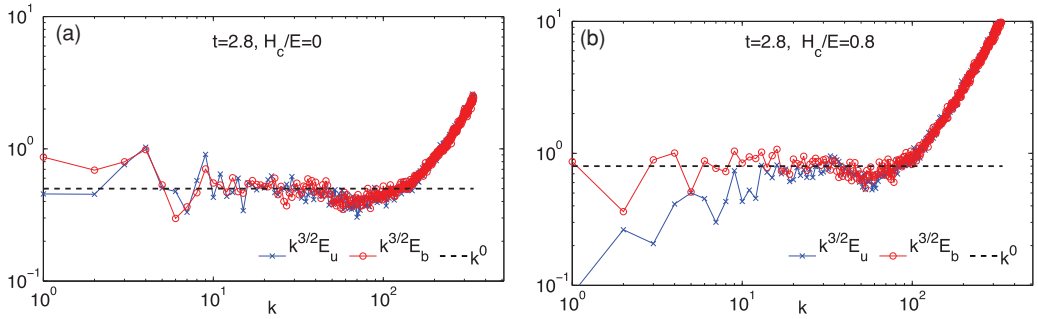

FIG. 4. (Color online) Energy spectra for random initial conditions with normalized velocity-magnetic field correlation of 0 (a) and 0.8 (b); kinetic (×, blue) and magnetic (circle, red) spectra are compensated by $k^{3/2}$. The dashed lines correspond to an IK spectrum, with $C_{IK} = 0.8$ (a) and $C_{IK} = 0.5$ (b), see Eq. (22).

The kinetic and magnetic energy spectra, compensated by a $k^{3/2}$ power law, are shown in Fig. 3 for several times, in the range $t \sim 2.5$ to $t \sim 20$, with blue ×'s for $E_u(k)$ and red circles for $E_b(k)$. As in the case of thermalization for the truncated Euler equation evolution in hydrodynamics with large-scale initial conditions, a clear scale separation now appears in these spectra.

It is possible then to define a wave number $k_{\rm th}(t)$ where the thermalized k^1 power-law zone starts [numerically determined by seeking the minimum of $E(k)$]. The total thermalized energy and enstrophy are thus defined as

$$E_{\rm th}(t) = \sum_{k_{\rm th}(t)}^{k_{\rm max}} E_T(k,t), \quad \Omega_{\rm th}(t) = \sum_{k_{\rm th}(t)}^{k_{\rm max}} \Omega_T(k,t). \qquad (20)$$

We now can estimate the effective energy dissipation rate as $\varepsilon_{\rm th}(t) = \frac{dE_{\rm th}}{dt}$. Similar to the 3D Euler case [8,9], this quantity presents a maximum, here for $t \approx 2.5$ (data not shown). Note that this time also corresponds to the interval of time during which the total dissipation, when viscosity and magnetic resistivity are added to the primitive equations, is quasistationary (see [25]). The scaling laws for a K41 spectrum (dotted line) and for the IK spectrum (dashed line), defined respectively as

$$E_u^{K41}(k) \approx E_b^{K41}(k) \sim C_K \varepsilon^{2/3} k^{-5/3} \qquad (21)$$

and

$$E_u^{IK}(k) \approx E_b^{IK}(k) = C_{IK} [\varepsilon b_{\rm rms}]^{1/2} k^{-3/2}, \qquad (22)$$

are also displayed in Fig. 3 at large scales, with $b_{\rm rms} \sim 2.5$ the root mean square value of the fluctuating magnetic field. The numerical constants C_K and C_{IK} appearing in front of the K41 and IK spectra are evaluated [see Fig. 3(a)] by fitting the large-scale part of the spectra at an early time after the first Alfvénic energetic exchange, $t \sim 2.5$ (note that the turbulence spectrum is already visible at $t \sim 2.0$, not shown). We find for these constants $C_K = 2$ and $C_{IK} = 0.8$ at the time of the maximum of the effective dissipation $\varepsilon_{\rm th}(t)$.

Therefore, we can safely conclude, on the basis of the examination of the results plotted in Fig. 3, that the IK spectrum is obtained in the intermediate spatiotemporal range of ideal dynamics in MHD in two dimensions for the OT vortex. Also note the good equipartition of kinetic and magnetic energy in the thermalized range, and the domination of magnetic energy at large scale, again a sign of a plausible inverse cascade associated with the magnetic potential.

B. Random initial conditions

Similar results obtain for random initial conditions, as can be seen in Fig. 4 plotting spectra in that case for a normalized global velocity-magnetic field correlation (H_c/E) that takes values of 0 (a) and 0.8 (b): A thermalized spectrum is observed at small scale, and a turbulent IK spectrum at large scale. However, note that nonuniversality has been obtained in MHD [16] in the three-dimensional decaying dissipative case, with either a K41, IK, or weak turbulence spectrum depending on the initial conditions for the magnetic field and with identical velocities and ideal invariants. A K41 spectrum was also previously obtained in decaying 2D MHD turbulence with random initial conditions using a Lagrangian model [26]. Moreover, in a similar study of ideal 2D MHD also using random initial conditions [27], a K41 spectrum was identified at large scales, together with non-Gaussian statistics associated with current and vorticity structures at intermediate times.

C. The pseudodissipative range, or lack thereof

Note that the end of the pseudoinertial range is not followed by a sharp decrease in energy before the thermalized $E_T(k) \sim k$ small-scale spectrum, contrary to the 3D Euler case [8,9]. However, computing a dissipation wave number using the IK spectrum and the corresponding evaluation of the transfer time that leads to the IK spectrum gives $\ell_{\rm diss} \sim \nu^{2/3}$, where in our ideal case the viscosity is replaced by a turbulent expression based on the thermalized energy, $\nu_{\rm turb} \sim \sqrt{E_{\rm th}}/k_{\rm max} \sim 1/k_{\rm max}$. Similarly, one can recall that the eddy viscosity computed with the EDQNM (eddy-damped quasinormal Markovian) closure gives a nonzero contribution [28]. However, several remarks are in order. First of all, the small-scale velocity leads to no contribution to an eddy viscosity for the dynamics of the large-scale velocity field [5], so the sole contribution to dissipation of E_u will stem from the small-scale magnetic field. Furthermore, the eddy resistivity contributions of the small-scale velocity and magnetic field exactly compensate each other when $E_u = E_b$ in the small scales, which is the case here (with small β). However, one can compute the correction to equipartition which is known to follow a k^{-2} law in the dissipative case [29]; therefore, one

could expect a nonzero contribution to turbulent viscosity in 2D MHD as well. Finally, another argument can be put forward to explain the lack of sharp decrease of the spectra before the thermalized range, namely that there are not enough modes in quasiequilibrium to produce a sufficient amount of effective dissipation. Indeed, in the 3D case, it was shown that a number of roughly 256^3 modes was necessary to see this internal decrease of the energy spectrum before the thermalized spectrum; this would correspond to a computation on a grid of 4096^2 points in 2D. However, observe that using a resolution of 2048^2 points, a slight dissipative zone seems to appear at $t = 2.3$ (for $k \approx 50$). This point will await further study.

To try to understand further the lack of dissipation range, we also resorted to an examination of the two-dimensional Euler case that is given in some detail in the Appendix. The truncated Euler equations relax toward the statistical equilibrium in an analogous way to the three-dimensional case. The main difference is the presence of a direct cascade of enstrophy. This quantity plays the role of the energy in 3D, thermalizing in equipartition at large wave number and yielding a k^{-1} law in the inertial zone. Again, a remarkable difference with the 3D Euler case is the absence of a dissipative zone that is likely due here to a vanishing 2D eddy viscosity.

IV. DYNAMICAL SLOWING DOWN IN THE PRESENCE OF A UNIFORM MAGNETIC FIELD

In the presence of a strong imposed uniform magnetic field of amplitude b_0, it is known that the dynamics is slowed down, including in the ideal case [23]; this is in fact at the basis of the argument of Iroshnikov and Kraichnan for an energy spectrum in MHD different from the Kolmogorov spectrum, and it is the feature on which the weak turbulence development for MHD relies [15], using the smallness of the ratio of the Alfvén time to the eddy turnover time:

$$R_{WT} = \tau_A/\tau_{NL}, \tag{23}$$

with $\tau_A = L_0/b_0$ and $\tau_{NL} = L_0/U_0$, L_0 and U_0 being respectively the characteristic large scale and velocity of the flow. It is also claimed in [23], in the framework of ideal 2D MHD, that in fact the development of small scales in the presence of a sufficiently strong $\mathbf{b}_0$ is arrested, with a smallest excited scale ℓ_B that depends on $\mathbf{b}_0$ and that can be larger than the smallest resolved scale of the flow in a computation at a given resolution.

In view of the increased power of computers available today, we revisit the effect a uniform field has on the formation of small scales in the ideal case of 2D MHD. Compared to the work in [23], we are now performing computations for longer times, for different values of the magnetic field b_0, and for higher resolutions, using here grids up to $N^2 = 4096^2$ points.

In Fig. 5 we give the temporal evolution of two modes, one in the middle of the resolved range ($k = 13$), and the other one at the end ($k = k_{\max} = N/3$), both normalized by $E(k = 1, t = 0)$, and for several values of the imposed field (see caption for symbols and colors). We observe a delay in the early dynamics of the modes as b_0 increases, followed at long times by a saturation once equilibrium is reached [particularly so for $E(k_{\max})$].

The logarithmic decrement technique [30] is now applied to quantify further the delay of the onset of the evolution as

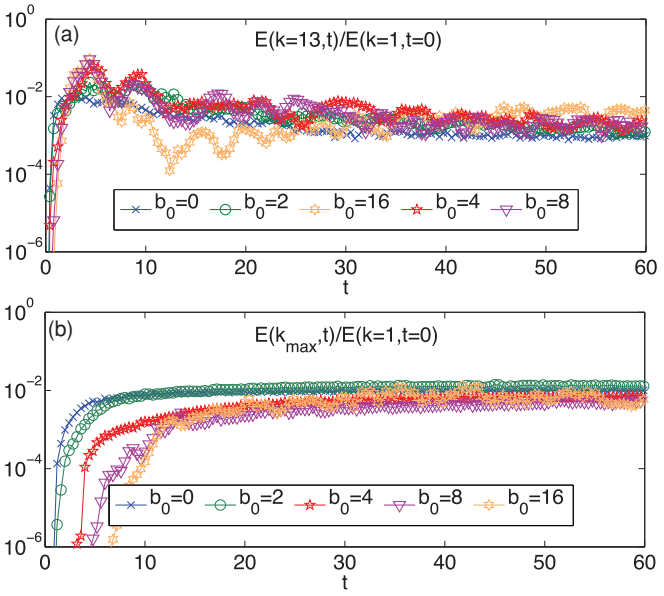

FIG. 5. (Color online) Temporal evolution of total (kinetic plus magnetic) energy in mode $k = 13$ (a) and $k = k_{\max}$ (b) for several imposed mean fields, both modes being normalized by the initial energy in the gravest mode: $b_0 = 0$ ($\times$, blue), $b_0 = 2$ (circle, green), $b_0 = 4$ ($*$, red), $b_0 = 8$ (triangle, purple), and $b_0 = 16$ (star, yellow). Note the substantial delays in the evolution as b_0 increases, and the final saturation level. Grids of 512^2 points (run 2, see Table I).

the amplitude of the imposed uniform field is increased. If the fields are regular, then the energy spectra must decay at least exponentially at large wave number k. Based on this assumption, the logarithmic decrement $\delta(t)$ is defined by the large k asymptotic of the energy spectra:

$$E_T(k) = c(t)k^{-m(t)}e^{-2\delta(t)k}; \tag{24}$$

$\delta(t)$ is measured by fitting the long wave-number range and the minimum admissible value is determined by the relation $\delta(t)k_{\max} = 2$ ($\delta =$ twice the mesh). The temporal evolution of $\delta(t)$ for different values of the imposed magnetic field is displayed in Fig. 6(a) in a log-lin plot.

The presence of a strong magnetic field slows down the nonlinear interactions and $\delta(t)$ remains above the minimum admissible value for a longer time the stronger the value of $\mathbf{b}_0$, as displayed in Fig. 6(a); the symbols for the different magnitudes of the imposed filed b_0 are identical to the preceding figures. It finally reaches the condition $\delta(t)k_{\max} = 2$ near $t = 3$ for $b_0 = 4$ (and $t \sim 5.8$ for $\mathbf{b}_0 = 8$). From this study, we can deduce that the system can reach statistical equilibrium even in the presence of a strong imposed magnetic field, but that the convergence toward such a state is considerably hampered. In Fig. 6(b), we also display the temporal evolution of the kurtosis for the current (darker color or shade of gray) and vorticity (lighter color or shade of gray) and for several imposed uniform magnetic fields. Again, the delay in the formation of small scales is observed, as well as a tendency toward Gaussianity once the thermalization takes place.

It may appear somewhat surprising that a different conclusion is reached with the present data from what is argued in [23] on the basis of a quasiregular behavior of MHD in two dimensions in the presence of a large-scale magnetic

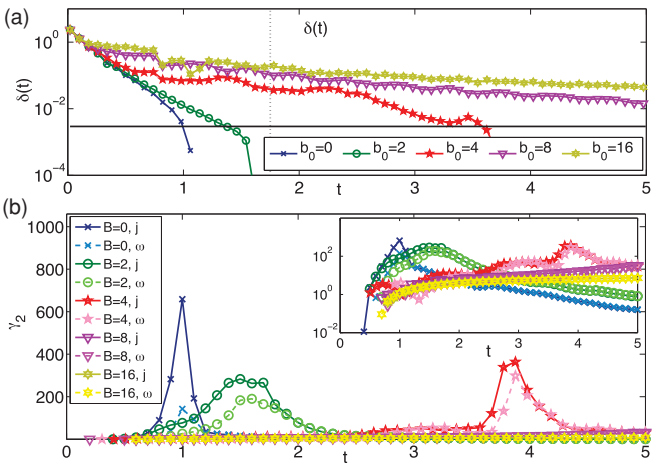

FIG. 6. (Color online) (a) Temporal evolution of the logarithmic decrement $\delta(t)$ with $b_0 = 0$ (blue $\times$), $b_0 = 2$ (green circle), $b_0 = 4$ (red star), $b_0 = 8$ (purple triangle), and $b_0 = 16$ (yellow $*$). Resolution of 2048^2 grid points, runs 3 and 4 of Table I. The horizontal solid line gives the smallest admissible value of δ for the PDEs to be well resolved for these grids, and the vertical dashed line represents the time at which integration was stopped in [23] for a computation on a grid of 256^2 points. No saturation of the temporal evolution of the logarithmic decrement $\delta(t)$ is observed provided the numerical resolution allows one to compute for long enough times. (b) Kurtosis $\gamma_2 = \kappa_4/\kappa_2^2$ (with κ_i the cumulant of order i) for the same runs as above, of the current j and vorticity ω for different values of the background constant magnetic field; the current is shown with a solid line (and darker color or shade of gray), whereas the vorticity is given with a dashed line (and lighter color). In the inset is given the same plot in log-lin coordinates. Note the change of shades (darker for j, lighter for ω, see inset on the left) in (b).

field: Indeed, such a field retards the nonlinear dynamics and can be seen as a bath of weakly interacting Alfvén waves with a spectrum that can be derived analytically in the case of a strong enough b_0, using weak turbulence theory [15]. However, it is well known that the weak turbulence approach is nonuniform in scale: The small parameter of the problem, R_{WT}, should be evaluated taking into account that the eddy turnover time gets smaller as smaller scales are reached, whereas the length scale of the imposed field remains infinite, by construction. Working out this relation in the case of the IK spectrum, $E(k) \sim (\epsilon b_0)^{1/2} k^{-3/2}$ leads to a scale $\ell_B \sim 1/b_0$ with $R_{WT}(\ell_B) = 1$, a scale beyond which a classical small-scale turbulent spectrum will develop; it should be noted, however, that the resolution of the computation must be such that ℓ_B is reachable accurately ($2\ell_B k_{\max} > 1$) in order to observe this phenomenon.

We now examine numerically the spectral temporal relaxation to equilibrium; several times are displayed in Fig. 7, with dashed lines corresponding to a k^{+1} scaling, and with the symbols and colors for different b_0 as before. We first observe that, at early times, the spectra coincide at large scales, but that small-scale thermalization is delayed for stronger imposed fields.

At intermediate times, there is a domain of wave numbers in which the dynamics differs quite substantially according to the value of $\mathbf{b}_0$. It appears that there is now a relaxation to equilibrium at intermediate wave numbers (the k^1 scaling law seems to be followed, see the figure) before a sharp plunge in the spectrum due to the fact that small scales are not reached yet because of the substantial slowing down of the dynamics. This is particularly striking at $t \sim 5$ for which the run with the largest value of the imposed mean field already presents a partial thermalization at intermediate wave numbers, as if the dynamics was indeed seeing a truncation at wave numbers much lower than the actual $k_{\max}$ of the run, whereas for $\mathbf{b}_0 = 4$, energy continues to flow to smaller scales. At a later time ($t \sim 15$), the $\mathbf{b}_0 = 4$ case now may be seeing a pseudotruncation in scale and partially thermalizes at intermediate scales, but it still cannot reach the smallest scales numerically available to the run. At the final time of the computation, $t \sim 60$, the three

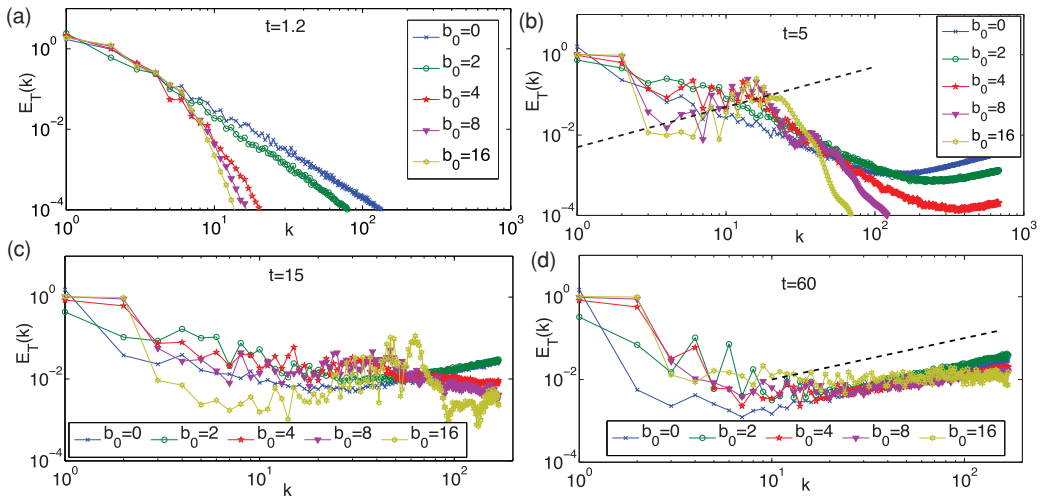

FIG. 7. (Color online) Total energy spectra with $b_0 = 0$ (blue $\times$), $b_0 = 2$ (green circle), $b_0 = 4$ (red $*$), $b_0 = 8$ (purple triangle), and $b_0 = 16$ (yellow star) at $t = 1.2$ and $t = 5$ [(a) and (b), with a grid of 2048^2 points, runs 3 and 4 of Table I], and $t = 15$ and $t = 60$ [(c) and (d), grid of 512^2 points, run 2]. The dashed lines correspond to an ideal k^1 scaling. Thermalization may occur for very long times at high b_0, but the spectral index at intermediate scales and times for higher b_0 is far from the predicted value, with possibly a partial thermalization at these intermediate scales [see (b)].

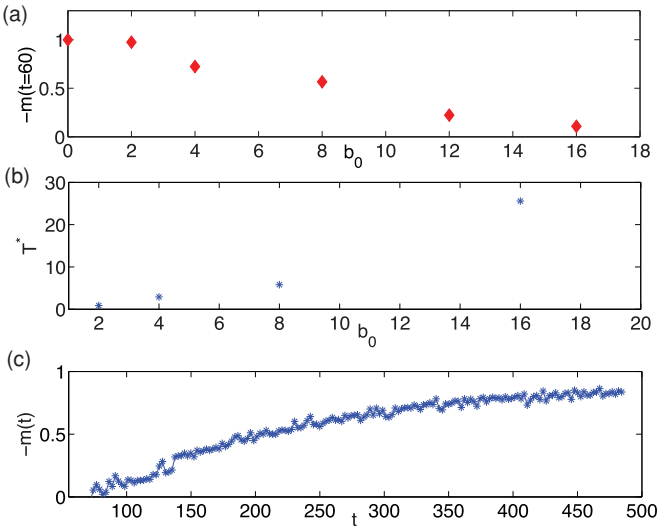

FIG. 8. (Color online) Variations with imposed mean field b_0. (a) Spectral index $\alpha = -m$ [see Eq. (24) with $\delta(t) \equiv 0$] of the thermalized part ($k \geqslant 20$) of the total energy spectra at $t = 60$ (see Fig. 7) for several b_0. Orszag-Tang vortex, resolution of 512^2 grid points, run 2 (see Table I). (b) Time T^* as a function of b_0; T^* is defined as the time at which the grid size is reached by the computation, as measured by the logarithmic decrement δ. (c) Temporal evolution of the spectral index for $k \geqslant 20$ with an imposed uniform field $b_0 = 16$ at resolution 256^2 (run 1); note the slow evolution toward the expected equilibrium value of $\alpha = 1$.

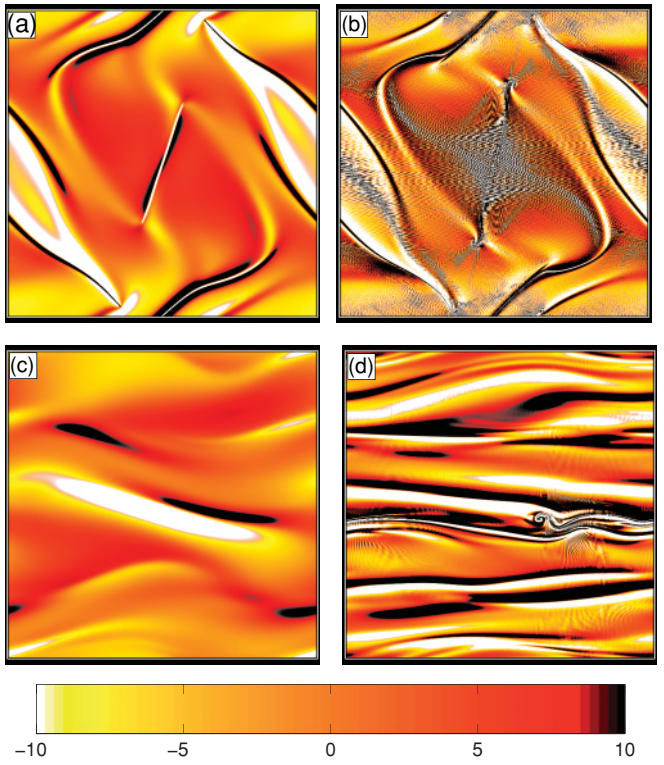

FIG. 9. (Color online) Density plot of current. (a) Current for $b_0 = 0$ at $t = 0.9$ (resolution of 4096^2 grid points). (b) Current for $b_0 = 0$ at $t = 1.1$ (resolution 4096^2). (c) Current for $b_0 = 4$ at $t = 1.1$ (resolution 2048^2). (d) Current for $b_0 = 4$ at $t = 3.7$ (resolution 2048^2). In the presence of even a moderate uniform field ($b_0/b_{\rm rms} \sim 2.8$ here), the onset of thermalization that destroys structures is delayed and the flows align themselves with b_0.

runs start to display thermalization in a broader range of scales, although the evolution of the gravest mode is quite retarded again compared to the weak field case. However note that the exponent of the thermalized zone clearly depends on $\mathbf{b}_0$ [see Fig. 8(a)]; for $\mathbf{b}_0 = 16$, the exponent is close to 0 indicative of a partial one-dimensional thermalization.

Figure 8(b) displays the time T_* at which the smallest effective excited scale in the flow reaches the grid size [$\delta(T_*) = 2/k_{\rm max}$]. Observe that T_* is an increasing function of b_0 and no sign of saturation of this slowing down is observed yet, although one might want to test higher values of b_0 as well. Including all points, a quadratic variation of T_* with b_0 is plausible. Note however that the close to zero value of the spectral index for $b_0 = 16$ [see Fig. 8(a)] is in apparent contradiction with the expected k^{+1} power law of equipartition of energy in 2D. It requires substantially longer times of integration to check whether the convergence toward the predicted statistical equilibrium is particularly slow or whether another solution is obtained (as in the Fermi-Pasta-Ulam-Tsingou problem [31]). In order to investigate this point, we performed an integration until $t = 475$ at moderate resolution. The spectral index for this run is displayed in Fig. 8(c) and it is found to asymptotically approach 1, the predicted value of the 2D absolute equilibrium.

V. STRUCTURES

The structures that develop in the flow we study here have been examined in detail in [23] at early time. Here, we pursue this study at higher resolution and examine how these structures change with $\mathbf{b_0}$ and with time. The structures are shown in Fig. 9 using grids of 2048^2 and 4096^2 points. At early times, the flows are made up of quasisingular structures which persist until $t \lesssim 1$ for $b_0 = 0$ [Figs. 9(a) and 9(b)] and for longer times when the magnitude of the external field is increased [see Figs. 9(c) and 9(d), obtained for the case $b_0 = 4$]. Once the thickness of these structures reach the grid size, noise steps in but the structures continue to evolve exhibiting some localized short-wavelength oscillations. These kinds of oscillations were already observed in the case of 1D Burgers and 2D incompressible truncated Euler equations [32]. It was argued that these oscillations come from resonant interactions between the fluid particle motion and waves induced by the truncation. As in the cases studied in Ref. [32], the localized structures observed in Figs. 9(b) and 9(d) invade the full domain until the system is able to reach complete thermalization. A further study of the formation of these MHD localized structures will be the subject of a future work.

In the presence of an imposed field, when strong enough, structures align themselves in its direction. Furthermore, the appearance of noise is clearly delayed; at a given time, it is not yet visible as the amplitude of b_0 increases (contrast the current at $t = 1.1$, for $b_0 = 0$ [Fig. 9(b)] and $b_0 = 4$ [Fig. 9(c)]). Finally, note that in all cases with strong imposed field, the small-scale structures display an intense folding and piling up of sheets of opposite signs.

VI. CONCLUSIONS

We have investigated in this paper the dynamics of an ideal two-dimensional fluid in the MHD limit, in the presence or not of a uniform magnetic field $\mathbf{b}_0$, and we have shown the link to the dissipative driven case. For $\mathbf{b}_0 \equiv 0$ and at intermediate times and intermediate scales, a behavior observed in the dissipative driven case obtains, namely, that the energy spectrum is that proposed by Iroshnikov and Kraichnan, with a $k^{-3/2}$ power law [13,14] for the Orszag-Tang vortex and for random flows, with in both cases initial conditions centered in the large scales. Furthermore, as already found in [23] but for shorter evolution times and lower resolutions, the formation of small scales is inhibited when $\mathbf{b}_0 \neq 0$.

Note that small-scale initial data was also studied in [33] where it was shown that the system reaches equilibrium by an eddy-noise mechanism. No inverse cascade was observed as the mechanism of thermalization. In the case of MHD an equipartition of magnetic potential leading to a k^3 scaling-law for the magnetic energy spectrum and k^1 equipartition for the kinetic energy spectrum was obtained at large times.

Extension of this work to the three-dimensional case in MHD may be of use for at least three reasons:

(i) It has been shown in [16] that, for initial conditions that are identical from the point of view of the statistics (same energy, same velocity field, same equipartition between kinetic and magnetic energy at $t = 0$, same large-scale-centered initial conditions, same total magnetic helicity, and with total velocity–magnetic field correlation between 0 and 4%, in normalized value), three different energy spectra could emerge in the absence of imposed uniform magnetic field and forcing (decay case with nonzero viscosity and unit magnetic Prandtl number) when considering three different initial conditions for the induction. Would they be observed as well at intermediate times–intermediate scales in the ideal case? It is plausible to think so, since a Kolmogorov spectrum is observed in the ideal 3D case for neutral fluids, and we observe the Iroshnikov-Kraichnan spectrum in the present work, but it would be of interest to verify the lack of universality in MHD in the ideal case as well.

(ii) Would a fast-decreasing spectrum at the end of the inertial range and before the thermalized range obtain in three-dimensional MHD, as it does in the 3D neutral case? It is argued in this paper that the lack of such a range is probably due to an insufficient number of thermalized modes because the total number of modes in two dimensions is not very large, compared to the three-dimensional case at the same linear resolution; thus, an effective eddy viscosity does not obtain here, and such a 3D computation would provide a test of this idea.

(iii) Finally, the case of magnetic helicity $H_M = \langle \mathbf{a} \cdot \mathbf{b} \rangle$, an invariant in ideal MHD in three dimensions, deserves a separate study. Indeed, it was shown in [29] that, performing a standard phenomenology à la Kolmogorov on H_M, the spectrum becomes $H_M(k) \sim k^{-7/3}$, but recent studies have shown that different spectra obtain [34–36] with $H_M(k) \sim k^{-3}$ or steeper. The origin of this discrepancy is not completely understood; it could be related to a detailed quasiequipartition between kinetic and magnetic modes in the energy and helicity parts of their spectral correlation functions. Again, an ideal study may help unravel the mechanisms at play in the dynamical evolution of MHD turbulence.

ACKNOWLEDGMENTS

Computer time was provided by IDRIS. The National Center for Atmospheric Research is sponsored by the National Science Foundation.

APPENDIX: THE FLUID CASE IN 2D

We take here as initial conditions $\mathbf{b} \equiv 0$, and for the stream function we have

$$\psi(x,y) = \frac{1}{k_a} \sin k_a x \sin k_a y + \frac{2}{k_b} \cos k_b x, \qquad \text{(A1)}$$

with the parameters set to k_a=1 and k_b=2. The temporal evolution of the enstrophy spectra is displayed in Fig. 10. As in 3D, a clear scale separation also appears: There is a progressive thermalization starting from the smallest scales, with the energy (vs enstrophy) cascading to the larger (vs smaller) scales. Note that the thermalized enstrophy increases from zero at early times to an amount of the order of the total enstrophy available in the system. Defining $k_{\rm th}$ as previously, and using the values of $\Omega_{\rm th}$ and $E_{\rm th}$, we can compute the parameters (Lagrange multipliers) α and β from

$$E(k) = \frac{2\pi k}{\alpha + \beta k^2}, \quad \Omega(k) = kE(k). \qquad \text{(A2)}$$

These Kraichnan absolute equilibria are displayed as solid lines at small scale in Fig. 10 (notice that they curve down at the larger scale of the thermalized zone for enstrophy); these solutions correspond to the k^3 scaling of the high enstrophy containing absolute equilibria.

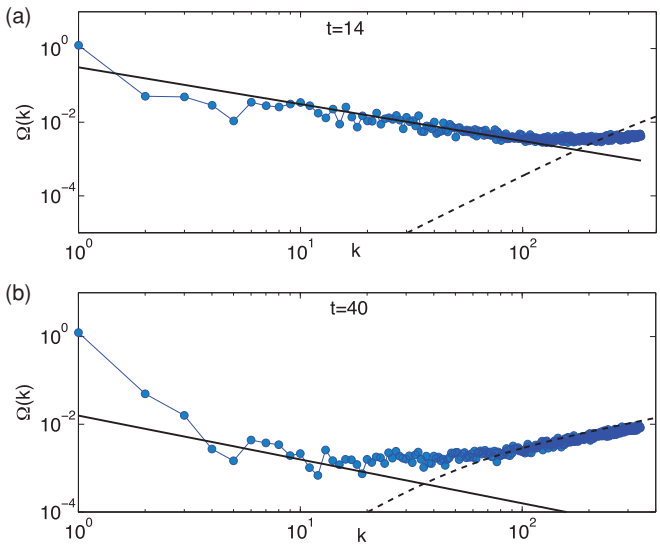

FIG. 10. (Color online) Temporal evolution of enstrophy spectra $\Omega(k) = k^2 E(k)$ for 2D Euler, at $t = 14$ (a) and $t = 40$ (b). Solid and dashed lines respectively indicate the enstrophy cascade (k^{-1} scaling) and thermalized enstrophy at small scales. Again note, as in the 2D MHD case, the absence of a pseudodissipative range before equipartition sets in.

The good agreement shows that the evaluation of $k_{\rm th}$ and the energy and enstrophy at the wave number describe reasonably correctly the temporal behavior of the flow (in the latter case, as $\eta_{\rm th}^{2/3}k^{-1}$). The enstrophy dissipation rate $\eta_{\rm th}$ can be estimated, defining it as the time derivative of $\Omega_{\rm th}$. The respective spectra are also displayed as solid lines at large scales in Fig. 10; observe that in the inertial zone both scaling law and prefactor are in good agreement with $\Omega(k) \sim \eta_{\rm th}^{2/3}k^{-1}$.

The relaxation dynamics of two-dimensional Euler turbulence is, *mutatis mutandis*, similar to the three-dimensional Euler case: a direct cascade of enstrophy (energy in 3D) followed by an equilibration of enstrophy (energy in 3D) at small scale. It can be shown [33] that the dissipation wave number estimated from the equilibria is of the order of the maximum wave number, thereby explaining in this case the absence of dissipation range as a buffer zone between the inertial range and the thermalized range, contrary to the 2D MHD case.

[1] L. Onsager, Nuovo Cimento **6** (Suppl. 2), 279 (1949).
[2] T. D. Lee, Quart. J. Appl. Math. **10**, 69 (1952).
[3] W. H. Matthaeus and D. Montgomery, *Proceedings of the Scientific Computer Information Exchange Conference* (Lawrence Livermore Laboratory, 1979).
[4] R. H. Kraichnan, Phys. Fluids. **10**, 1417 (1967).
[5] R. H. Kraichnan and D. Montgomery, Rep. Prog. Phys. **43**, 547 (1980).
[6] U. Frisch, A. Pouquet, J. Léorat, and A. Mazure, J. Fluid Mech. **68**, 769 (1975).
[7] A. Pouquet, in *Astrophysical Fluid Dynamics*, edited by J. P. Zahn and J. Zinn-Justin, *Proceedings of the Les Houches Summer School, XLVII, 1987* (Elsevier, 1993), pp. 139–227.
[8] C. Cichowlas, P. Bonaiti, F. Debbasch, and M. E. Brachet, Phys. Rev. Lett. **95**, 264502 (2005).
[9] G. Krstulovic, P. D. Mininni, M. E. Brachet, and A. Pouquet, Phys. Rev. E **79**, 056304 (2009).
[10] P. D. Mininni, P. Dmitruk, W. H. Matthaeus, and A. Pouquet, e-print arXiv:1005.1574.
[11] G. Krstulovic and M. E. Brachet, Physica D **237**, 2015 (2008).
[12] P. Goldreich and S. Sridhar, Astrophys. J. **438**, 763 (1995).
[13] P. S. Iroshnikov, Soviet Astronomy **7**, 566 (1964).
[14] R. H. Kraichnan, Phys. Fluids **8**, 1385 (1965).
[15] S. Galtier, S. Nazarenko, A. Newell, and A. Pouquet, J. Plasma Phys. **63**, 447 (2000).
[16] E. Lee *et al*., Phys. Rev. E **81**, 016318 (2010).
[17] S. A. Orszag, in *Fluid Dynamics*, edited by R. Balian and J. L. Peube, *Proceedings of the Les Houches Summer School, 1973* (Gordon and Breach, New York, 1977).
[18] D. Fyfe and D. Montgomery, J. Plasma Phys. **16**, 181 (1976).
[19] R. H. Kraichnan, Acoust. Soc. Am. **27**, 438 (1955).
[20] S. Ghosh and W. H. Matthaeus, Phys. Fluids B **2**, 1520 (1990).
[21] S. Ghosh and W. H. Matthaeus, Phys. Fluids A **4**, 148 (1992).
[22] S. A. Orszag and C. M. Tang, J. Fluid Mech. **90**, 129 (1979).
[23] U. Frisch, A. Pouquet, P.-L. Sulem, and M. Meneguzzi, J. Méc. Théor. Appl. **2**, 191 (1983).
[24] R. Bruno and V. Carbone, Living Rev. Solar Phys. **2** (2005).
[25] H. Politano, A. Pouquet, and P. L. Sulem, Phys. Fluids B **1**, 2330 (1989).
[26] P. D. Mininni, D. C. Montgomery, and A. G. Pouquet, Phys. Fluids **17**, 035112 (2005).
[27] M. Wan *et al*., Phys. Plasmas **16**, 080703 (2009).
[28] A. Pouquet, J. Fluid Mech. **88**, 1 (1978).
[29] A. Pouquet, U. Frisch and J. Léorat, J. Fluid Mech. **77**, 321 (1976).
[30] C. Sulem, P. L. Sulem, and H. Frisch, J. Comput. Phys. **50**, 138 (1983).
[31] E. Fermi, J. Pasta, and S. Ulam, LASL Report LA-1940, 1955.
[32] S. S. Ray, U. Frisch, S. Nazarenko, and T. Matsumoto, Phys. Rev. E **84**, 016301 (2011).
[33] G. Krstulovic, Ph.D. thesis, Université Paris VI, 2010 [http://tel.archives-ouvertes.fr/tel-00505813/fr/].
[34] W. C. Müeller (private communication); see also S. Malapaka and W.-C. Müller (unpublished).
[35] P. D. Mininni and A. Pouquet, Phys. Rev. E **80**, 025401 (2009).
[36] S. K. Malapaka, Ph.D. thesis, University of Bayreuth, Germany, 2009.